ЖЭТФ/JETP, 2026, том 170, вып. 6 (12), стр. 625–630 © 2026

EFFECT OF SPIN-ORBIT INTERACTION ON PHYSICAL PROPERTIES OF SnAs SUPERCONDUCTOR

V. A. Vlasenko, **M. D. Alien***

P. N. Lebedev Physical Institute of the Russian Academy of Sciences
Moscow, 119991, Russia

Received July 21, 2026,
revised version September 14, 2026
Accepted for publication September 18, 2026

In this work, the effect of spin-orbit coupling (SOC) on the electronic structure, electron-phonon spectrum, and superconducting properties of the NaCl–type (rock-salt) compound SnAs is investigated via ab initio calculations. Inclusion of the SOC provides only a minor influence on the equilibrium lattice parameter and the electronic density of states near the Fermi level. However, it produces a notable restructuring of the high-frequency region of the electron-phonon spectrum and the Eliashberg spectral function $\alpha^2F(\omega)$, which in turn modifies the electron-phonon coupling constant. The calculated coupling parameter λ_{el-ph} equals approximately 0.59 when SOC is taken into account and 0.63 when it is neglected. The superconducting critical temperature Tc, obtained within the Migdal-Eliashberg formalism, lies in the range 3.1–4.1 K, depending on the chosen parameter of smearing for the Eliashberg function and on whether SOC is incorporated. These findings underscore the necessity of explicitly including spin-orbit coupling for a quantitatively accurate theoretical description of the superconducting state in SnAs.

Keywords: superconductivity, spin-orbit coupling, electron-phonon interaction, Eliashberg spectral function

DOI: 10.31857/S0044451026120099

1. INTRODUCTION

It is well known that the binary 11-family compounds SnTe, SnSe, and SnAs crystallize in the rock-salt (NaCl–type) structure. These materials display a remarkably diverse range of physical properties, including topological-insulator behavior, magnetism, and superconductivity [1]. Within this family, SnAs is a superconductor. Transport measurements show that, above its superconducting transition temperature of 3.5–4.2 K [2–4], SnAs exhibits typical Fermi-liquid metallic behavior [5]. Thermodynamic studies together with nuclear magnetic resonance (NMR) experiments further establish that SnAs is a type-I superconductor with a critical field H_c of 280–400 Oe [2, 6]. Structurally, SnAs adopts a cubic lattice with $Fm\bar{3}m$ space group with a primitive unit cell containing one As atom at the $4a$ $(0, 0, 0)$ Wyckoff site and one Sn atom at $4b$ $(0.5, 0.5, 0.5)$, see Fig. 1. A main particularly noteworthy feature is its excellent structural compatibility, along the [111] direction, with tin-based layered compounds of the 122 family—such as $EuSn_2As_2$ (Eu-122), $CaSn_2As_2$, and $SrSn_2As_2$ (Sr-122). These 122 compounds exhibit topologically nontrivial electronic states, superconductivity, and magnetism, rendering SnAs as highly promising platforms for heterostructure engineering [7–9].

Recent first-principles studies indicate that SnAs may realize a topological semimetal phase characterized by pronounced band splitting, and also has been proposed as a candidate for topological superconductivity [6]. Numerical calculations of the physical properties of SnAs reported in the literature [3,6,10] have provided comprehensive results for its electronic, electron–phonon, and mechanical properties. In particular, the influence of spin–orbit coupling on the electronic band structure was examined in Ref. [3]. However, all previously published first-principles studies of the superconducting properties of SnAs were performed without inclusion of spin–orbit coupling [5,10,11]. Therefore, in the present work we have carried out a systematic ab initio investigation of the effect of spin–orbit coupling on the superconducting properties of SnAs.

* E-mail: vlasenkovlad@gmail.com

2. METHODS

First-principles (*ab initio*) calculations were performed within the framework of density functional theory (DFT) using the plane-wave pseudopotential method, as implemented in the Quantum ESPRESSO (QE) package [12]. Electron–electron exchange–correlation interactions were described by the generalized gradient approximation (GGA) in the Perdew – Burke – Ernzerhof (PBE) parametrization. The kinetic-energy cutoff for the wave functions was set to 120 Ry (1 Ry $\approx$ 13.605 eV), while the charge-density and potential cutoff was fixed at 700 Ry. Brillouin-zone sampling was carried out on a $24 \times 24 \times 24$ Monkhorst–Pack k-point mesh. The phonon properties and the electron–phonon coupling matrix elements were obtained within the density functional perturbation theory (DFPT) [13]. Integration over the Fermi surface employed a smearing technique with a Gaussian broadening parameter of $\sigma = 0.01$ Ry. A $12 \times 12 \times 12$ Monkhorst – Pack k-point grid was used for the Brillouin-zone integration of the electron–phonon quantities. Dynamical matrices were computed on uniform from $2 \times 2 \times 2$ up to $6 \times 6 \times 6$ q-point meshes.

3. RESULTS AND DISCUSSION

First, structural relaxation calculations (vc-relax) were iteratively performed using the Quantum ESPRESSO package to optimize the unit cell volume and atomic positions. The resulting refined cubic lattice constants were determined to be $a_{\text{nsoc}} = 5.807$ Å in the absence of spin-orbit coupling (SOC) and $a_{\text{soc}} = 5.808$ Å with SOC included. For comparison,

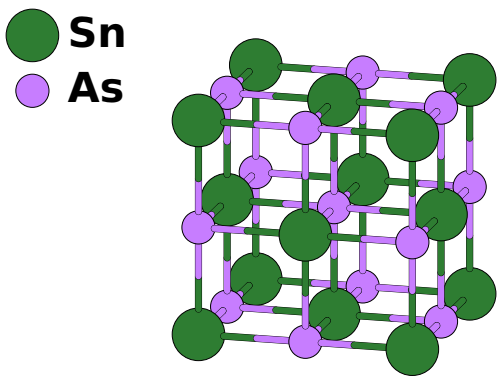


Fig. 1. Crystal structure of the SnAs superconductor with the NaCl-type structure

Table 1. Calculated lattice parameter values depending on the choice of pseudopotential

Pseudopotential	a (Å)
PAW (SOC)	5.80773
ONCVP (SOC)	5.80724
USPP (SOC)	5.80788
ONCVP (nSOC)	5.8075
USPP (nSOC)	5.8087
PAW (nSOC)	5.8084

the experimental lattice parameter a_{exp} ranges from 5.72 to 5.725 Å [2,14,15]. Consequently, the calculated lattice constants are approximately 1% larger than the experimental values. This slight overestimation has been observed in previous studies [15] and is independent of the pseudopotential choice (see Table 1). It may be attributed to lattice compression in real crystals caused by strain accumulation due to crystal structure defects.

The electronic band structure and density of states (DOS) presented in Fig. 2, exhibit a metallic or semimetallic character [10, 16], irrespective of whether SOC is included. Notably, the DOS near the Fermi level E_f is almost unaffected by SOC. The calculated DOS values at the Fermi level, $N(E_f)$, are 0.620 eV/state and 0.617 eV/state without and with SOC, respectively. This relatively low $N(E_f)$ implies a modest superconducting critical temperature T_c [10] and a small electron-phonon coupling parameter, in accordance with the relation [17, 18]:

$$\lambda_{e-ph} = -\frac{N(E_F)\langle I^2\rangle}{M\langle\omega^2\rangle}, \tag{1}$$

where M is the average atomic mass, $\langle\omega^2\rangle$ is the mean-square phonon frequency, and $\langle I^2\rangle$ is the Fermi-surface-averaged squared electron-phonon interaction [19]. According to this relation, the electron-phonon coupling constant λ increases linearly with $N(E_f)$.

Angle-resolved photoemission spectroscopy (ARPES) observations indicate that at least one band crosses the Fermi surface, while theoretical calculations suggest the presence of several pockets, implying multiband conductivity in SnAs [3, 16]. From the obtained electronic DOS, the Sommerfeld coefficient γ can be estimated as $\gamma = \frac{\pi^2}{3} N_a k_b^2 N(E_f) \approx 1.45 \frac{\text{mJ}}{\text{mol}\cdot\text{K}^2}$ (SOC) and $1.44 \frac{\text{mJ}}{\text{mol}\cdot\text{K}^2}$ (nSOC). Using the experimental value $\gamma = 2.18 \frac{\text{mJ}}{\text{mol}\cdot\text{K}^2}$ [5], the effective electron mass ratio can be derived from: $\frac{\gamma_{\text{exp}}}{\gamma_{\text{cal}}} = \frac{m^*}{m_e} = 1.50$ (SOC), 1.51 (nSOC) These values

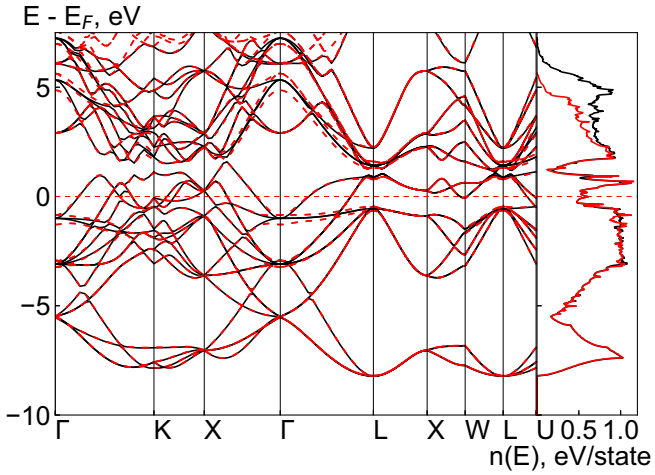


Fig. 2. Electronic band structure without SOC (black curves) and with SOC (red lines) together with the density of states (DOS) for both cases

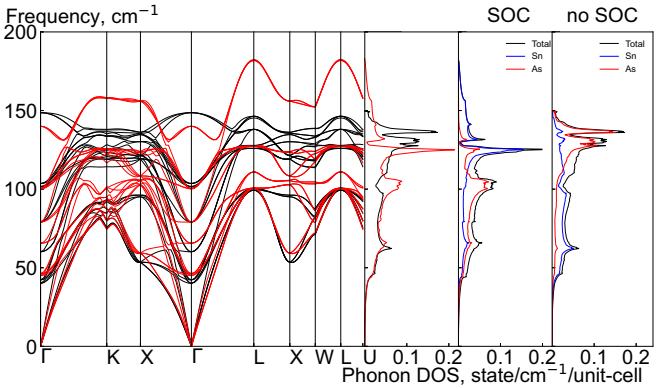


Fig. 3. Phonon dispersion for SnAs along the principal high-symmetry directions in the Brillouin zone with (red curves) and without (black curves) SOC together with the corresponding phonon density of states (PhDOS)

are in good agreement with previously published data [10, 20].

The superconducting properties of SnAs were investigated within the Migdal–Eliashberg framework [21, 22]. As noted above, the ab initio calculation of the phonon spectrum and phonon DOS was performed using the DFPT approach implemented in Quantum ESPRESSO. The results are presented in Fig. 3, where optical and acoustic modes are clearly resolved. Arsenic (As) atoms contribute predominantly to the high-frequency part of the spectrum, while tin (Sn) atoms dominate the low-frequency vibrations. The phonon spectra obtained without SOC are consistent with those reported in previous studies [6, 10].

The influence of SOC on the low-frequency part of the spectrum is negligible. However, in the high-frequency region, a notable restructuring of the spectral density is observed. Specifically, the phonon DOS without SOC exhibits two main maxima at approximately 130–135 cm^{-1}. Inclusion of SOC leads to a spectral redistribution, resulting in a single dominant peak at around 120 cm^{-1} and an additional feature at about 100 cm^{-1}. Consequently, the inclusion of SOC is expected to have a discernible impact on the calculated physical properties of SnAs.

From the calculated phonon spectra, the Eliashberg function $\alpha^2F(\omega)$ and the electron-phonon coupling constant were obtained (see Fig. 4) according to the following formulas:

$$\alpha^2F(\omega) = \frac{1}{N_q N_F} \sum_{q\nu} \frac{\gamma_{q\nu}}{\omega_{q\nu}} \delta(\omega - \omega_{q\nu}), \tag{2}$$

$$\lambda_{e-ph} = \int_0^{\omega_{\max}} \frac{2\alpha^2F(\omega)}{\omega}\, \mathrm{d}\omega, \tag{3}$$

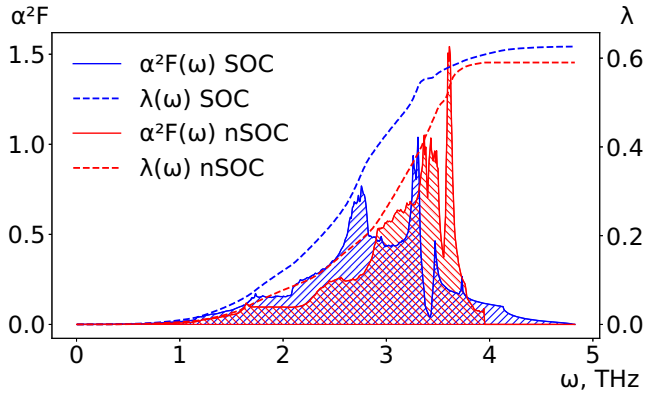


Fig. 4. Eliashberg spectral function $\alpha^2F(\omega)$ and the integrated electron-phonon coupling constant λ_{e-ph} for SnAs with and without SOC

where N_F and N_q are the density of states per spin at the Fermi level and with momentum q, respectively, and $\gamma_{q\nu}$ is the phonon linewidth (full width at half maximum).

As evident from the figure, the Eliashberg function inherits the shape of the phonon density of states. The integrated electron-phonon coupling constant λ_{e-ph} increases nearly parabolically across the entire frequency range, indicating comparable contributions from both acoustic and optical phonons to λ_{e-ph} [10]. The computed values are $\lambda_{e-ph} = 0.63$ and 0.59 with and without SOC, respectively. These relatively low values of the electron-phonon coupling constant are characteristic of conventional low-temperature superconductors, such as aluminum (Al) with $\lambda_{e-ph} \sim 0.44$ and $T_c \sim 1.2$ K, and palladium (Pd) with $\lambda_{e-ph} \sim 0.5$ and $T_c \sim 5.4$ K [23], etc.

This places SnAs within the weak-coupling regime and is well consistent with the Bardeen–Cooper–Schrieffer (BCS) model. Moreover, no signatures of unconventional superconductivity are observed in SnAs, while the estimated $2\Delta/T_c \approx 3.48 - 3.73$ ratio is close to the BCS value in the weak-coupling limit [3].

The critical temperature was estimated using the Allen – Dynes modification of the McMillan formula [18]

$$T_c = \frac{\omega_{\log} f_1 f_2}{1.2} \exp\left[\frac{-1.04(1+\lambda_{e-ph})}{\lambda_{e-ph}(1-0.62\mu^*)-\mu^*}\right] \quad (4)$$

Here, $\omega_{\log}$ is the logarithmically averaged frequency, f_1 and f_2 are the correction factors, and μ^* is the Coulomb pseudopotential. An estimate of μ^* can be obtained from the relation given in Ref. [24]:

$$\mu^* = \frac{0.26N(E_F)}{(1+N(E_F))} \quad (5)$$

When the density of states at the Fermi level is nearly identical regardless of SOC, the μ^* values are also expected to be essentially identical. We therefore adopt $\mu^* \approx 0.1$ in both cases. Using the calculated logarithmically averaged frequencies $\omega_{\log} = 137.4$ K and 152.7 K, and $\omega_2 = 148.9$ K and 162.4 K, obtained with and without SOC, respectively, and taking the Coulomb pseudopotential $\mu^* = 0.1$ [24], the superconducting critical temperature was evaluated. According to the Allen – Dynes formula, T_c was found to be 3.66 ± 0.8 K and 3.42 ± 0.8 K for the $12 \times 12 \times 12$ k-point and $4 \times 4 \times 4$ q-point grid, with and without SOC, respectively. These values are in good agreement with experimental results, which range from 3.58 K to 3.80 K [3, 5]. Additional calculations performed on other q-point grids and with criteria for evaluating T_c are presented in the Appendix (Figs. 5, 6).

Furthermore, according to the relation [25]:

$$\frac{\gamma'_{\rm sp} T_c^2}{H_{c2}^2(0)} = 0.168\left[1 - 12.2\left(\frac{T_c}{\omega_{\log}}\right)^2 \ln\left(\frac{\omega_{\log}}{3T_c}\right)\right], \quad (6)$$

where

$$\gamma_{\rm sp} = \frac{2}{3}\pi^2 k_B^2 n(\epsilon_F)(1+\lambda_{e-ph}-\mu^*), \quad (7)$$

Table 2. Summary of the superconducting properties of SnAs

	a (Å)	λ_{e-ph}	T_c, K	$\gamma_{\rm sp}$, $\frac{\rm mJ}{\rm molK^2}$	H_c, Oe
SOC[1]	5.808	0.63	3.66	1.45 2.63	327
nSOC[1]	5.807	0.59	3.4	1.44 2.55	299
[2]	5.72*	–	3.65 *	–	–
[3]	5.723*	–	3.60 3.8*	2.67* 1.89**	275**
[4]	5.721*	–	4.2*	–	81* 485*
[5]	5.725*	0.62*	3.58*	2.18*	172*
[6]	5.722*	0.66* 0.67**	3.74* 3.56**	2.59*	187*
[10]	5.812**	0.64**	3.24**	2.41**	–
[11]	5.684**	0.62**	3.08**	1.49**	–
[15]	5.864**	–	–	–	–
[20]	–	0.62**	–	1.49**	–

[1] present work, * experimental, ** ab initio.

the Sommerfeld coefficient γ and the upper critical field H_c can be estimated. For $\mu^* = 0.1$, the obtained values were $\gamma_{\rm sp} = 2.63 \pm 0.1$ mJ·mol^{-1}·K^{-2} and $\gamma_{\rm sp} = 2.55 \pm 0.1$ mJ·mol^{-1}·K^{-2} with and without SOC, respectively, while the critical field H_c was found to be 327 Oe and 299 Oe, respectively.

The Debye temperature can be estimated from the mean phonon frequency using the relation $\langle\omega^2_{\rm log}\rangle = 0.5\Theta^2_D$ [26], resulting values of Θ_D(SOC) $\approx$ 194 K and Θ_D(nSOC) $\approx$ 216 K. An estimate of Θ_D can also be obtained by inverting the McMillan equation:

$$\lambda_{e-ph} = \frac{1.04 + \mu^* \ln(\Theta_D/1.45T_C)}{(1 - 0.62\mu^*)\ln(\Theta_D/1.45T_C) - 1.04}. \quad (8)$$

Substituting the calculated values gives Θ_D(SOC) $\approx$ 168 K and Θ_D(nSOC) $\approx$ 190 K. It should be noted that some previous studies [5, 11] employed a Coulomb pseudopotential parameter $\mu^* = 0.13$ without explicit justification. In the present work, using $\mu^* = 0.13$ leads to a significant underestimation of the critical temperature; its adoption therefore appears unjustified for SnAs. A summary of the superconducting properties obtained in the present work and in previous studies is presented in Table 2.

4. CONCLUSIONS

For the first time, the influence of spin-orbit coupling on the phonon spectrum and the ensuing physical properties of the SnAs superconductor has been systematically investigated by means of ab initio methods. It is demonstrated that spin-orbit coupling induces a pronounced restructuring of the high-frequency region of the electron–phonon spectrum and provides an additional contribution to the electron–phonon coupling constant and, consequently, to superconductivity. The estimated critical temperatures range from 3.4 to 4.1 K, depending on the computational grid and the inclusion (or omission) of spin-orbit coupling; these values are in a good agreement with experimental data.

APPENDIX

In cases where an unrelaxed crystal structure with experimental a_{exp} values is used, a shift of the Eliashberg spectrum toward higher frequencies and a significant decrease in the electron-phonon coupling parameter are observed. These changes lead to a significant reduction in the calculated T_c value, which is considerably lower than the experimentally observed ones (see Fig. 5, 6).

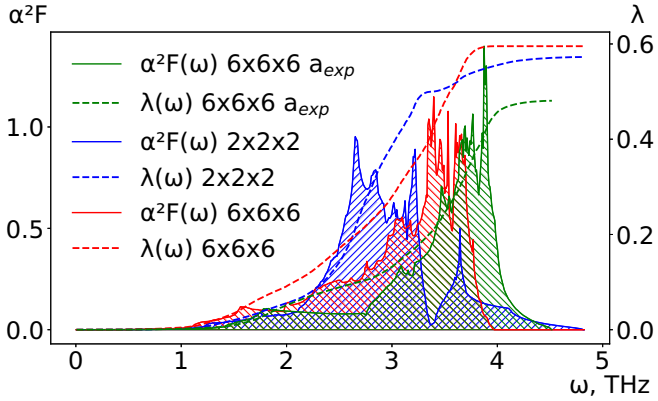


Fig. 5. Eliashberg spectral function $\alpha^2{\rm F}(\omega)$ and the integrated electron-phonon coupling constant $\lambda_{\rm e-ph}$ for SnAs without SOC, obtained from electron-phonon calculations on $2\times2\times2$, $4\times4\times4$, and $6\times6\times6$ q-point grids, respectively

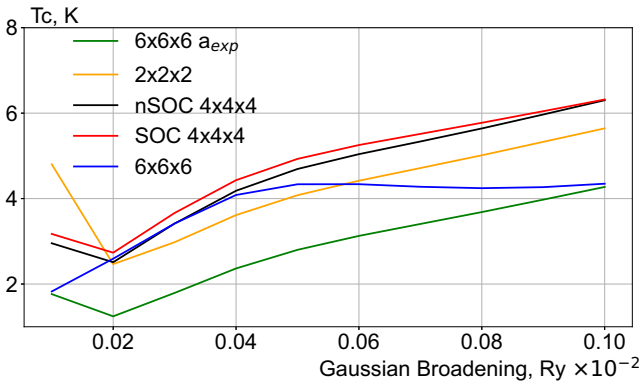


Fig. 6. Dependence of the critical temperature on the broadening of the delta peaks in the Eliashberg function for SnAs on a $4\times4\times4$ q-point grid with (red line) and without (black line) SOC, on a $2\times2\times2$ q-point grid (orange line), and on a $6\times6\times6$ q-point grid (blue line) and $6\times6\times6$ q-point grid and the experimental lattice parameter (green line), for $\mu^* = 0.1$

Acknowledgements. The work was performed using equipment of the Lebedev Physical Institute's Shared Facility Center.

Funding. The work was not sponsored.

Conflicts of interest. The authors declare that they have no conflicts of interest.

Author's contributions. The contributions of the authors are equal.

REFERENCES

1. L. D. Zhao, S. H. Lo, Y. Zhang et al., Nature (London) **508**, 373 (2014).

2. S. Geller and G. W. Hull Jr, Physical Review Letters **13**, 127 (1964).

3. P. I. Bezotosnyi, K. A. Dmitrieva, A. V. Sadakov et al., Physical Review B **100**, 184514 (2019).

4. M. M. Sharma, N. K. Karn, P. Sharma et al., Solid State Communications **340**, 114531 (2021).

5. Y. Wang, H. Sato, Y. Toda et al., Chemistry of Materials **26**, 7209 (2014).

6. S. Srivastava, O. Kulkarni, D. Singh et al., arXiv preprint arXiv:2512.17282 (2025).

7. V. A. Vlasenko, B. I. Massalimov, K. S. Pervakov, Bulletin of the Lebedev Physics Institute **53**, 96 (2026).

8. H. Li, W. Gao, Z. Chen et al., Physical Review B **104**, 054435 (2021).

9. K. Inzani, A. Faghaninia, S. M. Griffin, Physical Review Research **3**, 013069 (2021).

10. H. M. Tütüncü and G. P. Srivastava, Solid State Communications **221**, 24 (2015).

11. V. Kanchana, V. Reddy, T. E. Kanchana et al., Physica B: Physics of Condensed Matter (2017).

12. P. Giannozzi, O. Baseggio, P. Bonfà et al., The Journal of Chemical Physics **152** (2020).

13. S. Baroni, S. De Gironcoli, A. Dal Corso et al., Reviews of Modern Physics **73**, 515 (2001).

14. J. He, X. Zhang, X. Lai et al., Journal of Solid State Chemistry **252**, 106 (2017).

15. M. A. Rahman, U. K. Chowdhury, T. H. Bhuyan et al., Am. J. Condens. Matter Phys. **6**, 27 (2016).

16. P. I. Bezotosnyi, K. A. Dmitrieva, S. Y. Gavrilkin et al., JETP Letters **106**, 514 (2017).

17. P. B. Allen, Physical Review B **6**, 2577 (1972).

18. P. B. Allen and R. C. Dynes, Physical Review B **12**, 905 (1975).

19. H. L. Skriver and I. Mertig, Physical Review B **32**, 4431 (1985).

20. I. Hase, K. Yasutomi, T. Yanagisawa et al., Physica C: Superconductivity and its Applications **527**, 85 (2016).

21. G. M. Eliashberg, Sov. Phys. JETP **11**, 696 (1960).

22. A. B. Migdal, Sov. Phys. JETP **7**, 996 (1958).

23. S. Y. Savrasov and D. Y. Savrasov, Physical Review B **54**, 16487 (1996).

24. K. H. Bennemann and J. W. Garland, AIP Conference Proceedings American Institute of Physics **4**, 103 (1972).

25. J. P. Carbotte, Reviews of Modern Physics **62**, 1027 (1990).

26. W. L. McMillan, Physical Review **167**, 331 (1968).